Experimental study of vibrational excitation of allene by slow electron impact: Vibronic coupling in the shortlived negative ion states

Michael Allan

Citation: The Journal of Chemical Physics **100**, 5588 (1994); doi: 10.1063/1.467126
View online: http://dx.doi.org/10.1063/1.467126
View Table of Contents: http://scitation.aip.org/content/aip/journal/jcp/100/8?ver=pdfcov
Published by the AIP Publishing

Experimental study of vibrational excitation of allene by slow electron impact: Vibronic coupling in the short-lived negative ion states

Michael Allan
Institut de Chimie Physique de l'Université Fribourg, Pérolles, 1700 Fribourg, Switzerland

(Received 22 September 1993; accepted 4 January 1994)

Vibrational electron energy loss spectra, vibrational excitation functions, and angular dependence of vibrational energy losses were measured in relative units for propadiene (allene, $H_2C=C=CH_2$) in an incident energy range up to 16 eV. Resonant excitation via the 2 eV resonance is not very selective; symmetric and antisymmetric C–C–C stretch, CH_2 twist and scissoring, CH stretch, and C–C–C bending are all excited. The antisymmetric C–C–C stretch and CH_2 twist are excited by Jahn–Teller activity of the degenerate ^2E resonance, the bending by vibronic coupling with higher lying resonances. The essential features of the excitation are qualitatively rationalized by a Hartree–Fock (HF)/6-31G* anion potential energy surface. Unspecific excitation of high vibrational levels, accompanied by detachment of slow electrons, is also observed to result from attachment of 2 eV electrons, and is rationalized as a consequence of temporary trapping of part of the nuclear wave packet on the bound (not autodetaching) part of the anion potential surface. Very broad resonance features are observed in the 2–16 eV range, mainly in the excitation functions of the C–H stretch and the CH_2 scissoring vibrations. A moderately broad resonance peak at 11.5 eV, observed in the excitation of the symmetric and antisymmetric C–C–C stretch vibrations, is assigned to two overlapping σ^* shape resonances. Absolute elastic cross sections are given for reference.

I. INTRODUCTION

Vibronic coupling permits the understanding of important phenomena in chemistry, namely structure changes, often accompanied by symmetry lowering, in excited and ionic species; and of nonadiabatic processes, the radiationless transitions between electronic states.[1] Vibronic coupling in short-lived resonance states is expected to be particularly interesting because of the short lifetime of the coupled states and the additional possibility of indirect vibronic coupling through continuum.[2] Allene (propadiene **1**) is particularly suitable in this respect. Already the *cation* $\mathbf{1}^+$ of this molecule has proven to be an interesting study case, since the Jahn–Teller effect (a special case of vibronic coupling) results in a spectacular shape of the first photoelectron band.[3] The present work is concerned with the vibronic coupling in the allene *anion* $\mathbf{1}^-$, permitting a discussion of the specific differences between the effect of removing an electron in the cation and the effect of adding an extra electron in the anion.

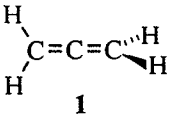

1

The ground state of the allene negative ion, corresponding to temporary occupation of the degenerate lowest unoccupied molecular orbital (LUMO) ^2E, was determined to lie at 1.9±0.1 eV by electron transmission spectroscopy (ETS).[4] Such states are short lived as a result of autodetachment, and are interchangeably called short-lived negative ion states, resonances, or negative ion resonances. The ground state of the allene anion is thus doubly degenerate and subject to Jahn–Teller distortion. Vibronic coupling with states resulting from electron capture to higher-lying molecular orbitals (MOs) is also possible and could lead to further distortion.

The lifetime of the short-lived anion formed by the attachment of an incident electron to the target molecule in resonant scattering is of the same order of magnitude as the vibrational period. The nuclei of the target molecule relax on the anion potential surface, causing vibrational excitation of the target molecule after the anion has eventually decayed back to the neutral molecule through autodetachment. Which vibrations have been excited is thus informative of the kind of distortion in the negative ion. The present work presents a comprehensive experimental study of vibrational excitation from threshold to 16 eV and discusses the results in the context of the electronic structure of the resonances and their relaxation dynamics.

II. EXPERIMENTAL SECTION

The electron energy loss spectrometer used in the present study has already been described.[5,6] It uses hemispherical electrostatic deflectors to prepare a beam of quasi-monoenergetic electrons and to energy analyze the scattered electrons. The analyzer is rotatable from −3° to 135° with respect to the incident beam and the instrument measures differential cross sections. The sample was kept at −80 °C and its vapor was introduced into the collision region as an effusive beam through a 0.25 mm nozzle, which was kept at 80±10 °C. The instrumental response function with respect to angle and electron energy was calibrated by comparing the elastic *e*-He signal with established calculated cross section values[7] as described previously.[5] All excitation functions and angular dependence spectra were corrected for this response function. The resolution (for energy-loss features) was 15 meV for the spectrum in Fig. 1, and 25 meV for the remaining energy loss and the energy- and angular-dependence spectra. The instrument is now equipped with an absolute pressure gauge in the inlet system and absolute elastic cross

 0021-9606/94/100(8)/5588/9/$6.00

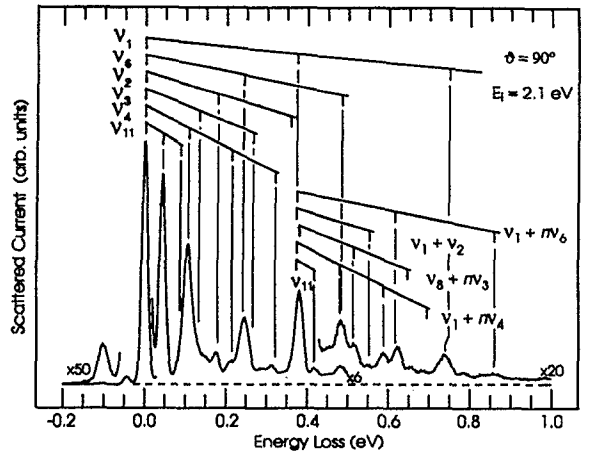

FIG. 1. Representative energy-loss spectrum excited by electrons with energies within the lowest ^2E resonance. Vibrational grids and vertical lines show selected standard vibrational energies from Table I, and their multiples and combinations, indicating a possible assignment of the observed features. (The little knick in the vertical line above $2\nu_1$ thus points out the size of anharmonicity.) Full discussion of the assignment is given in the text and in Table II.

sections have been determined using the relative flow technique as described by Nickel *et al.*[8]

III. RESULTS

A. The 2.0 eV LUMO resonance

Figure 1 shows an energy-loss spectrum recorded with an incident energy in the center of the LUMO resonance. The well-known vibrational frequencies of neutral allene[9] are listed in Table I. A unique assignment based on the vibrational frequency alone is not always possible with the present resolution and the possible assignments are summarized in Table II.

The peak at 44 meV is the most intense vibrationally inelastic peak and can be assigned unambiguously to the ν_{11} C–C–C bending vibration. Deciding which transition in ν_{11} is responsible for the $\Delta E = 44$ meV inelastic peak is complicated by the substantial thermal population of the doubly degenerate $1\nu_{11}$ level in the target molecule; about 25% of all molecules are in the $1\nu_{11}$ state and about 9% is in the $2\nu_{11}$ state at 80 °C. The inelastic peak at $\Delta E = 44$ meV is thus in majority due to the $n_{11}=0 \rightarrow n_{11}=1$ transition (where n_{11} designates the number of ν_{11} quanta excited in a given vibrational state), but with a significant contribution of the $n_{11}=1 \rightarrow n_{11}=2$ and even higher transitions. The ratio of intensities of the inelastic peak at $\Delta E = 44$ meV and the superelastic peak at $\Delta E = -44$ meV, equal to 4.5 in the spectrum of Fig. 1, is in good agreement with expectation based on the population of the $n_{11}=1$ and 2 vibrational states and the principle of detailed balancing. Similarly, transitions originating from the thermally populated $1\nu_{11}$ and $2\nu_{11}$ states must be contributing to the rest of the spectrum, which is discussed below. The number of ν_{11} quanta does not appear to change in these transitions, however, so that they overlap with the transitions originating from the vibrational ground state and do not visibly affect the spectrum. The role of the thermal population of the ν_{11} vibration will therefore not be mentioned explicitly in the subsequent paragraphs.

The next prominent peak, at 106 meV, can be assigned to the Jahn–Teller active mode ν_4 (107 meV), although a contribution of ν_{10} (104 meV) cannot be excluded. The 106 meV peak is clearly broader then the elastic peak, indicating the excitation of $2\nu_{11}$ on its left flank, and the excitation of ν_3 (or, less probably, of ν_9) on its right flank. The next clearly discernible peak, at 176 meV, can be assigned to CH_2 scissoring vibrations ν_2 or ν_7. The next prominent peak, at 245 meV, can be unambiguously assigned to the ν_6 antisymmetric C–C–C stretch vibration. The peak at 381 meV is broader than the elastic peak, indicating excitation of ν_1 (374 meV) and/or ν_5 (373 meV), and simultaneously of ν_8 (383 meV), all being C–H stretch vibrations. Assignments of several

TABLE I. Vibrational energies of allene taken from Ref. 9.

Symmetry species	No.	Energy (meV)	Approximate type of mode
a_1	ν_1	374	C–H symmetry stretch
	ν_2	179	CH_2 scissoring
	ν_3	133	C–C symmetry stretch
b_1	ν_4	107	CH_2 twist
b_2	ν_5	373	C–H stretch
	ν_6	243	C–C antisymmetry stretch
	ν_7	173	CH_2 scissoring
e	ν_8	383	C–H stretch
	ν_9	124	CH_2 rocking
	ν_{10}	104	CH_2 wagging
	ν_{11}	44	C–C–C deformation (bending)

TABLE II. Energies (in millielectron volts) and possible assignments of vibrational features excited by impact of 2.1 eV electrons (Fig. 1). Energy values in parentheses are inferred from overlapping peaks or shoulders and are less reliable. Literature values (Ref. 9) (and their combinations) of the vibrational frequencies are given in parentheses in the assignments column.

Energy	Possible assignments
−102	$-\nu_4(107)$ CH_2 twist, $-\nu_{10}(104)$ CH_2 wagging
−44	$-\nu_{11}(44)$ CCC deformation
0	Elastic peak
44	$\nu_{11}(44)$ CCC deformation
(86)	$2\nu_{11}(88)$
106	$\nu_4(107)$ CH_2 twist, $\nu_{10}(104)$ CH_2 wagging
(130)	$\nu_3(133)$ C–C stretch, $\nu_9(124)$ CH_2 rock
(144)	$\nu_6+\nu_{11}(148)$?
176	$\nu_2(179)$ CH_2 scissoring, $\nu_7(173)$ CH_2 scissoring
212	$2\nu_4(214)$, $2\nu_{10}(208)$
245	$\nu_6(243)$ antisymmetric C–C stretch
(290)	$\nu_6+\nu_{11}(287)$
313	$3\nu_4(321)$
381	$\nu_1(374)$, $\nu_5(373)$, $\nu_8(383)$ C–H stretch
420	$\nu_{11}+\nu_1(418)$
(453)	?
483	$\nu_1+\nu_4(481)$, $2\nu_6(485)$
515	$\nu_8+\nu_3(516)$
588	$\nu_1+2\nu_4(588)$
622	$\nu_1+\nu_6(617)$, $\nu_8+\nu_6(625)$
740	$2\nu_1(748)$, $3\nu_6(728)$

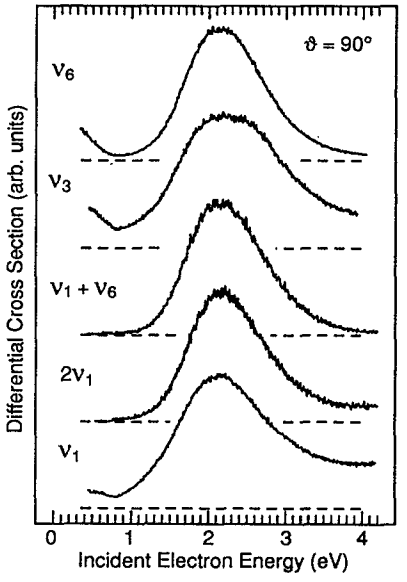

FIG. 2. Selected excitation functions in the region of the lowest ^2E resonance. Energy loss was held equal to the energy of the vibration indicated in the figure for each trace. The actual curve may have contributions from overlapping vibrations as indicated in Table II and in the text.

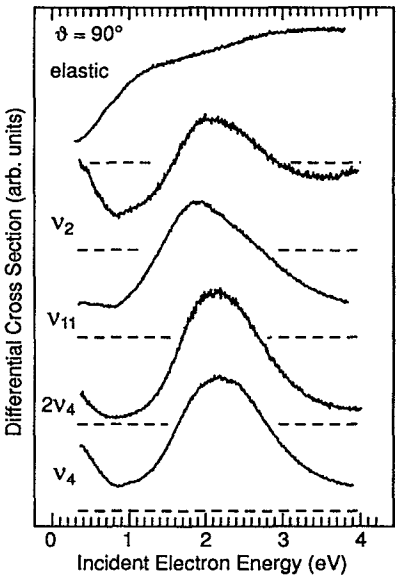

FIG. 3. See the caption of Fig. 2.

combination and overtone vibrations are also proposed in Table II and Fig. 1.

An important question concerns the excitation mechanism. The vibrations can be excited resonantly, a mechanism which is of interest here, but IR active vibrations (i.e., all except the a_1 vibrations) could also be excited directly through dipole interaction. The two mechanisms can be distinguished with the help of the dependence of the excitation on incident energy. The direct excitation mechanism is characterized by energy dependence peaking at threshold and decreasing monotonously with increasing energy; resonant excitation is enhanced at the energy of the resonance. Several excitation functions are given in Figs. 2 and 3. (No attempt has been made to deconvolute overlapping peaks; some of the curves are contaminated by a signal from overlapping peaks; the degree may be inferred from Fig. 1.) Signal increase with decreasing energy below 1 eV indicates direct excitation in most of the curves. It is evident, however, that the direct excitation makes a significant contribution only at energies below 1 eV for the fundamental vibrations, and becomes negligible at incident energies ~2 eV at a scattering angle of 90°. All vibrationally inelastic features in Fig. 1 are thus excited resonantly. Note that the rise of cross sections towards low energies is absent in the excitation functions of the $2\nu_1$ overtone and the $\nu_1+\nu_6$ combination vibrations (Fig. 2), which cannot be excited by the direct mechanism. The vibration ν_2 is not IR active, i.e., the signal rise towards threshold in the curve labeled ν_2 (Fig. 3) must be due to direct excitation of the overlapping IR active vibration ν_7. A second characteristic property of direct excitation is a rise of cross sections towards low scattering angles and will be discussed below.

The dipole excitation mechanism is illustrated by the energy-loss spectrum in Fig. 4, recorded at a residual energy of 0.5 eV, i.e., at incident energies below the 2 eV ^2E resonance, and at a low scattering angle. All observed peaks can be assigned to IR-active vibrations and the excitation of overtone and combination vibrations (e.g., in the 270–340 and 400–700 meV ranges) is, in contrast to the spectrum in Fig. 1, very weak.

Threshold peaks in vibrational cross sections have been the subject of numerous discussions in the literature. A matter of controversy (reviewed, e.g., in Ref. 10) has been their physical origin in a number of specific cases (HCl, CO_2, and CH_4), i.e., whether they are due to direct excitation through vibrating dipole moments at long range as discussed above, or whether they represent short range effects associated with "virtual states." The most important distinctions from the experimental point of view are the forward peaked cross section and applicability only to IR-active vibrations for the former mechanism, and nearly isotropic cross sections and

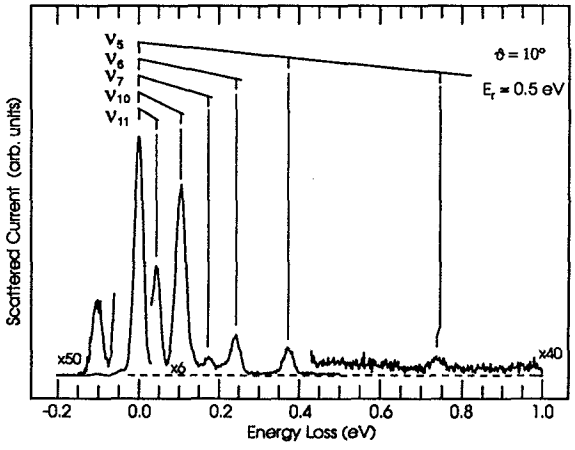

FIG. 4. Energy-loss spectrum recorded under conditions where direct excitation of IR active vibrations dominates. Note the absence (except weak $2\nu_1$) of overtone and combination vibrations.

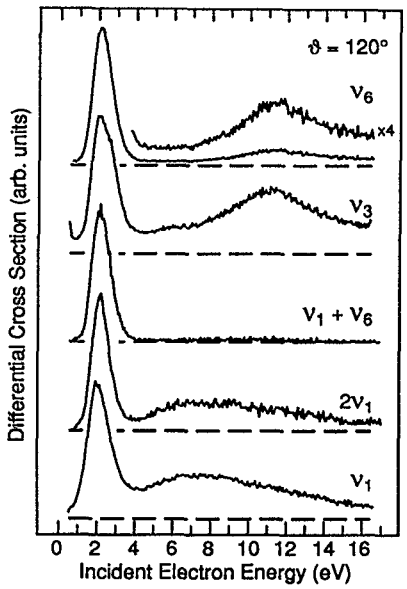

FIG. 5. Excitation functions recorded over a wider energy range, illustrating higher-lying resonances. The curves are labeled as in Fig. 2.

applicability also to totally symmetrical vibrations for the second mechanism. The threshold peaks observed in the present spectra of allene appear to be forward peaked and can all be explained as stemming from excitation of IR-active vibrations. The present spectra thus do not present a conclusive evidence for the necessity of including the concept of a virtual state at threshold in allene. The role of a virtual state cannot, on the other hand, be entirely excluded because of the overlap of IR-active and IR-inactive vibrations.

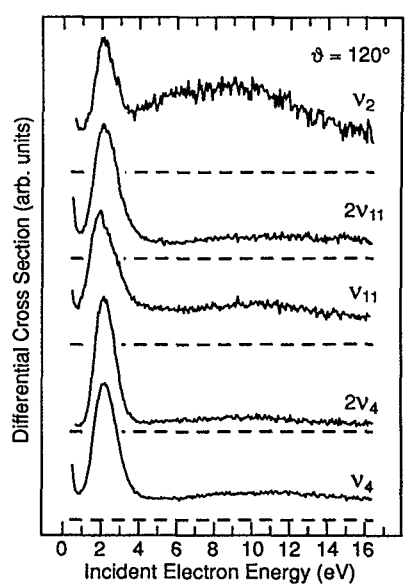

FIG. 6. See the caption of Fig. 5.

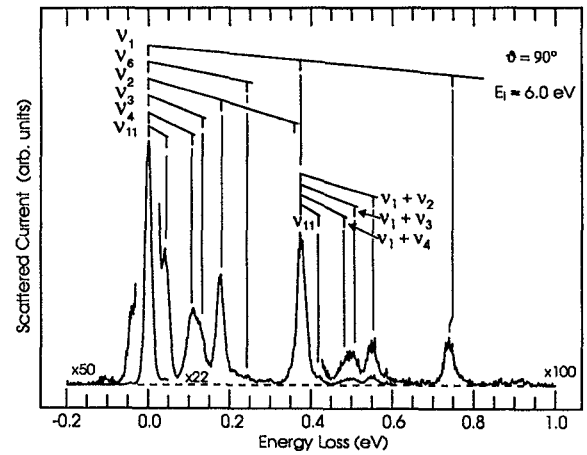

FIG. 7. Energy-loss spectrum illustrating vibrational excitation by the very broad resonances.

B. Higher-lying resonances

Several broad bands with distinctly selective excitation can be discerned in the 3–16 eV range in the excitation functions shown in Figs. 5 and 6. An extremely broad band peaking ~7 eV appears in the C–H stretch excitations at 379 meV (overlapping ν_1, ν_5, and ν_8) and their overtones at 742 meV. A similar very broad feature, albeit peaking at slightly different energies, appears in the ν_2 CH_2 scissoring and ν_4 twist vibration excitation functions. All these features overlap with the 2 eV ^2E resonance on the low energy side and consequently contribute to vibrational excitation even at 2 eV. Vibrational excitation in the 6 eV range is illustrated by the energy-loss spectrum in Fig. 7. The striking differences with respect to Fig. 1 are the dominant C–H stretch excitation, prominent ν_2 CH_2 scissoring excitation (both alone and in combination with ν_1), a near absence of the ν_6 antisymmetric C–C–C stretch vibration (again both alone and in combination with ν_1), and a relatively less prominent ν_{11} excitation. The C–H stretch band peaks at a slightly lower energy in Fig. 7 than in Fig. 1, indicating more ν_1 and little ν_8 excitation at 6 eV.

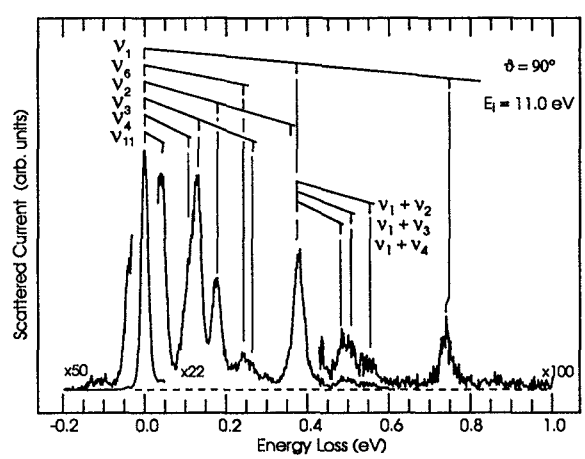

FIG. 8. Energy-loss spectrum illustrating vibrational excitation by the moderately broad 10–13 eV resonance.

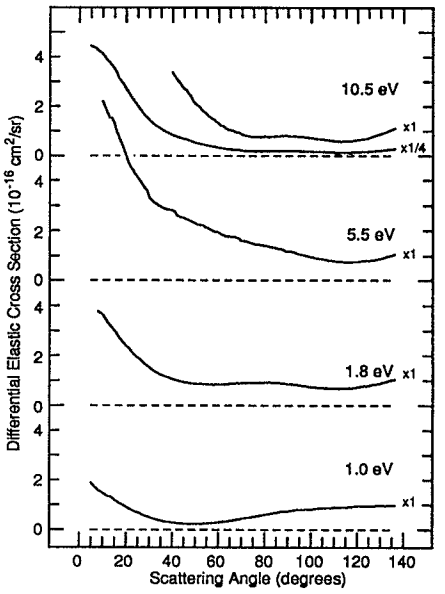

FIG. 9. Angular dependence of the elastic cross section at different energies. The absolute values are accurate within ±30%.

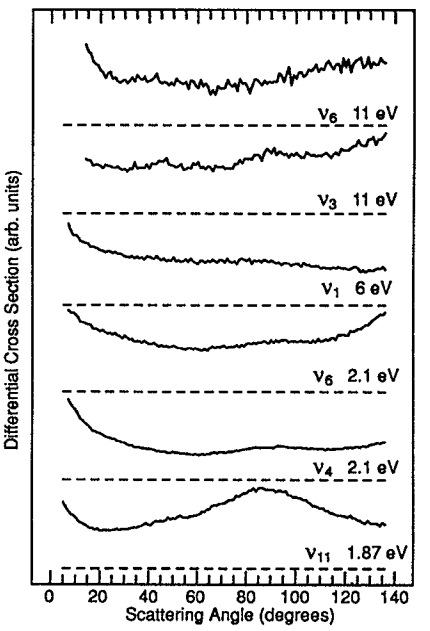

FIG. 10. Angular dependence of selected inelastic cross sections. The curves are not on the same vertical scale.

Finally, a moderately broad resonance peaking ~11.5 eV appears in the ν_3 symmetric and ν_6 antisymmetric C–C–C stretch vibrations. Vibrational excitation in this region is illustrated by the energy-loss spectrum in Fig. 8, which shows clearly the enhanced ν_3 symmetric and ν_6 antisymmetric C–C–C excitations in comparison with excitation at 6 eV in Fig. 7.

C. Angular distributions

Angular distributions of the vibrationally elastic cross sections are given in Fig. 9 and those of selected inelastic peaks are in Fig. 10. As in the case of energy dependence, some of the inelastic curves may contain a signal from overlapping peaks. The target molecules are to a significant degree thermally vibrationally excited as discussed above. The elastic cross section at 1.8 eV is somewhat reminescent of *d*-wave scattering, with a weak maximum near 90°, a behavior which could be due to the "π^*" character of the ^2E resonance in allene. Some of the inelastic cross sections, e.g., those of ν_{11} and ν_4 at 2.1 eV, exhibit a rise at low scattering angles, which can be attributed to direct excitation of IR active vibrations. The cross sections are not far from isotropic above 20°, indicating that the excitation is predominantly resonant at scattering angles above 20° and at incident energies above 2 eV. The inelastic cross sections do not show any pronounced single partial wave behavior, in accordance with an expectation for excitation of nontotally symmetric vibrations in the presence of vibronic coupling.[2]

IV. DISCUSSION

A. Assignment of resonances

Assignment of the observed resonances is attempted within the context of the Koopmans' theorem[11] by comparison with *ab initio* virtual orbitals, shown schematically in Fig. 11. The linear scaling relation used to calculate the estimated attachment energies was derived by a least squares fit of π^* resonance energies, but appears to be a useful guide in the resonance assignment even for the higher resonances. The 2.0 eV band in the vibrational excitation functions (Figs. 2 and 3) is doubtlessly associated with a capture of the incident electron to the degenerate pair of the "π^*" e orbitals. The scaled orbital energy of 2.0 eV is in excellent agreement with the experimental value.

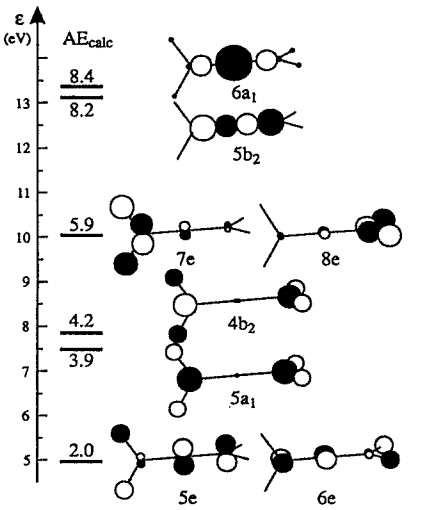

FIG. 11. Virtual orbitals of allene [calculated by the Gaussian 92 program (Ref. 16)]. 6-31G* orbital energies are indicated by heavy horizontal bars and the vertical scale on the left. Estimated attachment energies are calculated from the orbital energies using the linear scaling relation A.E.=(ϵ −2.33)/1.31 (in electron volts) (Ref. 12) and given in bold numbers above or below the horizontal bars. Schematic diagrams of 3-21G orbitals were drawn with the program MOPLOT (Ref. 13).

The application of Koopmans' theorem to the higher-lying, broad resonances may be questioned because of their large width. It is felt here, however, that the nodal properties of the virtual orbitals may be expected to resemble the nodal properties of the actual wave function in the vicinity of the target molecule and a qualitative comparison is revealing in the present case in the same sense as for the extremely short-lived and broad 3–6 eV resonance in H_2, which can be associated with the σ_u virtual orbital.[14] A second possible objection to the use of Koopmans' theorem is that extensive mixing (CM) of "shape" (one particle) and core excited (one hole, two particles) configurations is often found for higher-lying resonances, e.g., in benzenoid hydrocarbons.[15] A HF/6-31G* configuration interaction with singles (CIS) calculation of the excited states of the allene anion was carried out to estimate the extent of CM for the higher resonances. This calculation predicts several core excited resonances in the 7–12 eV incident energy range, but indicates a surprisingly low extent of mixing of shape and core excited configurations, thus adding justification to the use of the Koopmans' theorem. The core excited resonances are not expected to effect the pure vibrational excitation strongly. In addition, two excited states of the anion are calculated 8.8 and 9.3 eV above the anion ground state, i.e., at incident electron energies of 10.8 and 11.3 eV, whose description involves almost exclusively single configurations with the occupation of the $5b_2$ and $6a_1$ orbitals, indicating an assignment of the 10.5 eV band in Fig. 5 to B_2 and A_1 shape resonances.

Regarding Fig. 11, it may be noted that the $5a_1$, $4b_2$, $7e$, and $8e$ orbitals are strongly antibonding along the C–H bonds, and the $7e$ and $8e$ orbitals also are strongly antibonding along the H–H distance, and could thus explain the very broad features in the 3–15 eV range in the C–H stretch and CH_2 scissoring excitation in Figs. 5 and 6. The $5b_2$ and $6a_1$ orbitals explain well the 11.5 eV band in the excitation functions of the symmetric and antisymmetric C–C–C stretch vibrations (ν_3 and ν_6) in Fig. 5, since they are strongly antibonding along the C–C–C bonds. The absence of the 11.5 eV band in the C–H stretch and CH_2 scissoring excitation is also accounted for, since the $5b_2$ and $6a_1$ orbitals have nearly no amplitude on the H atoms. The antisymmetric C–C–C stretch vibration ν_6 cannot be excited by A_1 or B_2 resonances alone, but can be excited by vibronic coupling between them.

B. Vibrational excitation at 2 eV

The symmetric square of the E representation in the D_{2d} point group is $[E^2]=A_1+B_1+B_2$. The modes ν_1, ν_2, and ν_3 of A_1 symmetry may be excited according to the Condon principle; the modes ν_4, ν_5, ν_6, and ν_7 may be excited because of their Jahn–Teller activity in the degenerate ^2E state of the negative ion. Thus, already on the qualitative level, the prominent observed excitation of the ν_4 CH_2 twist and the ν_6 antisymmetric C–C–C stretch vibration indicates a pronounced Jahn–Teller activity of the 2 eV resonance. On the other hand, the very strong excitation of the C–C–C bend vibration ν_{11} indicates that vibronic interaction with higher resonances causes the allene anion ground state to be bent.

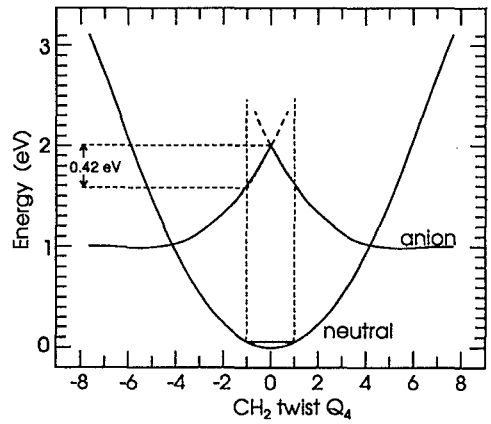

FIG. 12. HF/6-31G* energy of allene and UHF/6-31G* energy of the allene anion in the function of the twist normal coordinate Q_4 (of neutral allene). The origin of the energy scale is chosen at the minimum of the neutral allene potential and the anion curve is shifted to conform with the experimental attachment energy.

The degree to which vibrations will be excited depends on to which degree the nuclear wave packet will relax along the individual normal modes before the instant of detachment. Since the π^* orbital temporarily occupied in the 2 eV resonance is strongly antibonding along one C–C distance (Fig. 11), excitation of the antisymmetric and symmetric C–C–C stretches are well understood already on the qualitative level. Similarly, excitation of the twist vibration may be understood, since the twist allows a strong mixing of the occupied and the unoccupied initially degenerate e orbitals, resulting in stabilization. Some degree of CH_2 scissoring excitation can be understood as a result of the antibonding interaction between the hydrogen atoms in each CH_2 group in the e orbital (Fig. 11).

To gain a deeper, more detailed insight into the vibrational excitation, it is desirable to have at least a qualitative indication of the shape of the resonance potential energy surface. A full description of the nuclear dynamics requires a complex nonlocal potential, but this primarily experimental paper will be confined to a discussion of qualitative aspects using an estimate of the shape of the real part of the potential surfaces of the negative ion, obtained from *ab initio* calculations. This procedure is, strictly speaking, not applicable because the problem of an autodetaching negative ion is not variational, but qualitatively useful results are obtained when the extra electron is confined near the target molecule by a relatively small basis set. The 6-31G and 6-31G* basis sets were found to reproduce satisfactorily the π^* electron affinities using the Koopmans' theorem [plus an empirical scaling relation (see Fig. 11)] indicating that this basis set provides about the right degree of spatial confinement. The qualitative potential surfaces were therefore determined with the HF/6-31G and HF/6-31G* procedures, deliberately renouncing to higher levels of theory, which would be questionable in view of the fundamental limitations just mentioned. Both basis sets were found to give very similar results, and HF/6-31G* results will be discussed below.

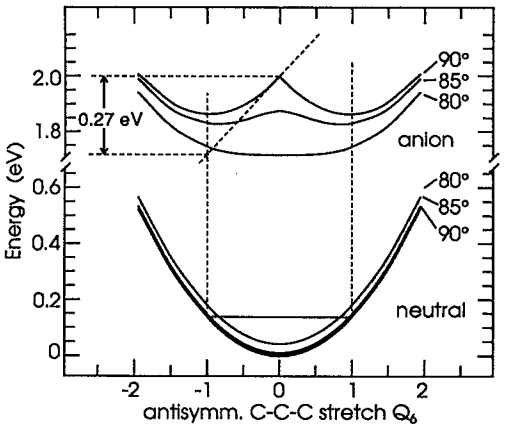

FIG. 13. The same as Fig. 12, but for the normal mode Q_6. The curves are drawn for three different values of the CH_2 torsion angle as indicated.

Examples of the potential energy dependence on three normal modes are shown in Figs. 12–14. The difference of self-consistent field (SCF) energies of the neutral and the anion is not a good indicator of attachment energy and the anion curves were thus shifted with respect to the neutral curves to conform with the experimental vertical attachment energy. The anion curves for the Jahn–Teller active modes in Figs. 12 and 13 show correctly a knick in the center, where the adiabatic curves cross, and a substantial slope along the normal modes Q_4 and Q_6, consistent with the strong excitation of the corresponding vibrations. The anion potential energy is calculated to descent as the anion is bent (Fig. 14), also in agreement with the observation. Interestingly, the slope of the anion potential surface as a function of Q_6 is calculated to diminish very rapidly when the torsion angle changes, i.e., the nuclear wave packet is predicted to relax along Q_6 and Q_4 initially, but the force along Q_6 vanishes quickly, as soon as the relaxation along Q_4 changes the torsion angle by only 10°. This effect will diminish the overall excitation of ν_6.

The slopes of the real part of the resonance potential surface with respect to the individual normal modes are related to the degree of excitation of individual vibrations by the impulse approximation.[14,17,18] It is applicable only for short lifetime resonances, and it is uncertain whether the lifetime of the ^2E resonance is sufficiently short to justify its application. The absence of vibrational structure in the energy dependence curves in Figs. 2 and 3 could be an indication of short lifetime, but could also stem from overlap of congested vibrational peaks. A comparison of calculated slopes and observed intensities may provide some useful insight, however, despite this uncertainty, and it is made in Table III. The slopes, in electron volts per unit of the dimensionless normal coordinate (defined to be equal to one at the classical turning points of the vibration) may be derived either graphically from the potential curves, as shown in Figs. 12 and 13, or, with the same result, from calculated Cartesian forces and normal mode displacements. The cross sections are proportional to the square of the slope for short-lived resonances.[18] The comparison should be made with integral cross sections, whereas the present experiment measures differential cross sections. A qualitative comparison with the peak heights in Fig. 1, which is made in Table III, is, however, also acceptable in view of the relatively flat angular distributions (Figs. 9 and 10). Only relative values are compared, and the squared slopes and experimental peak heights are therefore normalized at the highest inelastic peak, the CH_2 twist vibration ν_4. Very satisfactory agreement is then obtained for the antisymmetric C–C–C stretch vibration ν_6. The comparison for the symmetric C–C–C stretch vibration ν_3 is complicated by the overlap of the bands in the spectrum, but the observed signal appears to be weaker than the calculated expectation. The vibrations ν_1 and ν_5 (both C–H stretch), and similarly ν_2 and ν_7 (both CH_2 scissoring), cannot be distinguished in the spectrum and the intensity of the peak is therefore compared with the sum of the squares of the slopes in Table III. The observed intensity is clearly larger than the calculated expectation in both cases. A plausible explanation for this discrepancy can be seen in Figs. 5 and 6 (and similarly in Figs. 2 and 3). The broad resonance centered ~7 eV is very prominent both in the ν_1, ν_5 and in the ν_2, ν_7 excitation functions, overlaps with the 2 eV resonance, and contributes significantly to excitation even at 2.1 eV.

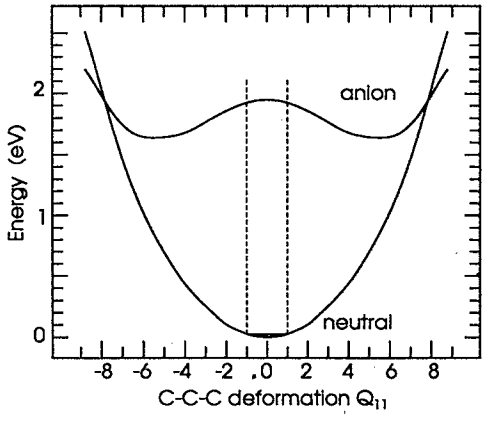

FIG. 14. The same as Fig. 12, but for the normal mode Q_{11}.

TABLE III. Slopes of the allene anion potential energy surface in the vicinity of the attachment point, calculated from UHF/6-31G* Cartesian forces and normal mode displacement. The forces are calculated at points slightly displaced (twisted or with unequal C–C distances) from the neutral allene geometry to avoid convergence problems. The slopes are in electron volts per unit of the dimensionless normal coordinate [defined to be equal to one at the classical turning points of the vibration (see also Figs. 12 and 13], as in Ref. 17. Slopes for ν_8–ν_{11} are zero. The second line gives the squares of the slopes, normalized to 1 for ν_4. The values for vibrations which cannot be resolved experimentally (ν_5 and ν_1, and ν_7 and ν_2) were summed. The last line gives the signal intensities measured at the energies of the vibrations in Fig. 1 (without attempts of deconvolution).

Vibration	ν_4	ν_6	ν_3	ν_5	ν_1	ν_7	ν_2
Slope	0.42	0.27	0.27	0.14	0.10	0.08	0.01
Normalized square	1.0	0.43	0.43	0.17		0.04	
Experimental intensity	1.0	0.48	(0.35)	0.68		0.23	

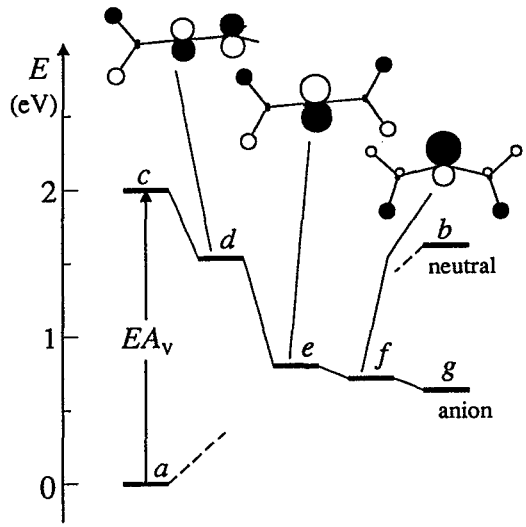

FIG. 15. A diagram of calculated energies of several structures of allene and its anion. The zero of the energy scale was set at the energy of neutral allene at its equilibrium geometry (a); the energy of the anion at the same geometry (c) was set to 2 eV using the experimental vertical electron affinity. The calculated HF/6-31G* stabilization of several structures of the anion is plotted relative to the energy (c). Relaxation of all C–C and C–H bond lengths (primarily prolonging the C–C bond along which is the temporarily occupied $5e$ orbital antibonding) and the C–C–H angles, but keeping the C–C–C structure linear and twist angle at 90° leads essentially to relaxation along the Jahn–Teller active antisymmetric C–C–C stretch mode Q_6, and results in a stabilization of about 0.45 eV (d). Relaxation of the twist angle leads to a substantially stabilized planar structure (e), with equal C–C bond lengths. Further stabilization is obtained by allowing the planar structure to bend (f). The equilibrium structure of the anion (g) is bent and slightly twisted. (b) is the energy of the neutral molecule at the equilibrium geometry of the anion, plotted relative to (a). Singly occupied orbitals are shown schematically [MOPLOT (Ref. 13)] for three anion structures.

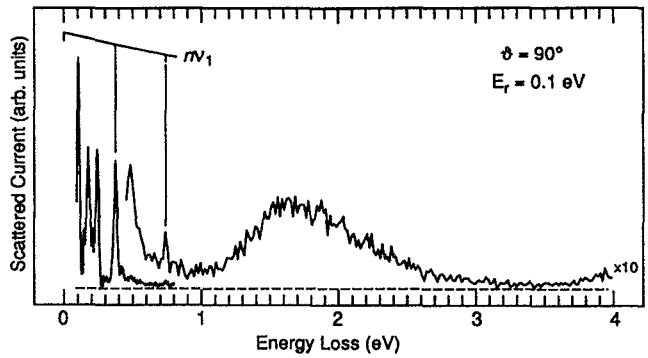

FIG. 16. Energy-loss spectrum recorded near threshold, with a constant residual energy of 0.1 eV. Discrete vibrational levels are excited at low energy losses, a quasicontinuum of vibrational levels is excited at the energy of the ^2E resonance in the 1.3–2.6 eV range.

The potential energy curve for the C–C–C deformation mode ν_{11} (Fig. 14) has a zero slope at the origin, so that excitation of double quanta of this vibration would be expected, caused by widening of the nucler wave packet along this normal mode coordinate on the anion potential energy surface. The prominent excitation of a single quantum of ν_{11} in the experiment (Fig. 1) indicates clearly that the adiabatic potential energy curve does not provide a complete description of the excitation in this case and that coupling with other states plays an essential role.

An impression of the potential surface shape further away from the equilibrium geometry of the neutral molecule, i.e., away from the point of attachment, is obtained by stepwise optimizing the geometry of the anion, starting at the geometry of the neutral molecule, as shown in Fig. 15. In the first step, the bending and twist were kept frozen, leading to an asymmetric relaxation of primarily the C–C distances, essentially along the symmetric stretch coordinate Q_3 and the Jahn–Teller active antisymmetric stretch Q_6. The twist angle was released in the next step, leading to a planar structure, with two equally long C–C bonds. This planar structure was then found to be further stabilized when allowed to bend. Finally, relaxing all degrees of freedom results in a slightly twisted bent structure of the allene anion with C_2 symmetry. This structure of the C_3H_4 anion was confirmed also with a larger basis set at the HF/6-311++G* level of theory, and including correlation, at the second-order Møller–Plesset (MP2)/6-31G* level.

The energies of neutral allene at its equilibrium geometry and the equilibrium geometry of the anion are also given in Fig. 15. The data sets for the neutral molecule and the anion were shifted relative to each other to reproduce the experimental electron affinity (E.A.) of 2.0 eV, similarly as in Figs. 12–14. Figure 15 indicates that the allene anion at its equilibrium geometry is stable towards autodetachment.

This means that part of the nuclear wave packet is expected to cross the stabilization point. The packet will not simply reflect on the outer slope as in the diatomic case, but may be trapped temporarily on the bound part of the potential energy surface through vibrational energy redistribution, spend a significant amount of time there, and cross the stabilization point (line) back to the autodetaching region from time to time. Most of the detachment during this time would thus occur close to the stabilization line, resulting in detachment of slow electrons. Such electrons are actually observed, as shown in Fig. 16. This represents a rationalization of the "unspecific" vibrational excitation mechanism in allene.

It is interesting that the 2 eV band in vibrational excitation has a slightly different shape in different final channels in Figs. 2 and 3. For example, the band appears relatively broad in the ν_3 symmetric stretch, the ν_4 CH_2 twist, and the ν_{11} C–C–C bending vibration, but narrower in the ν_6 antisymmetric stretch and most other channels. A faint indication of a double-peak shape may even be discerned in the ν_3 and ν_{11} channels, with a peak at 1.95 eV and a shoulder ~2.6 eV. This variety of shapes is not qualitatively surprising. The potential surfaces have a complex shape, of the same type as described for a model case by Estrada *et al.*,[2] with a square root intersection at the geometry of the neutral molecule and two potential surfaces V_+ and V_- around it. The transition during electron attachment is to some degree related to the transition to the also degenerate potential surfaces during ionization, where a double band structure was also found. The present situation is even more complicated because of the energy and nuclear coordinate dependent width of the potential surfaces. A qualitative rationalization of the de-

tailed shape of the 2 eV band in the excitation functions does not appear possible.

V. CONCLUSION

Resonant vibrational excitation via the 2 eV resonance in allene is not very selective, with the bending, symmetric and antisymmetric C–C–C stretches, CH_2 twist and scissoring, and at least two C–H stretch vibrations being excited.

Some aspects of the excitation are in qualitative agreement with expectation based on the calculated UHF/6-31G* potential energy surface. This suggests that such a potential surface, despite the fact that the problem is not variational in the autodetaching regions and the extra electron is held in the vicinity of the target by the modest size of the basis set, is useful to rationalize in part the behavior of the negative ion.

The problem of resonant vibrational excitation in allene at the energy of the first shape resonance is, however, decisively more complex and cannot be described by Jahn–Teller distortion and adiabatic potential curves only. Higher-lying σ^* resonances overlap with the π^* resonance because of their large width and substantially affect the excitation of CH_2 scissoring and C–H stretch vibrations even at the energy of the first resonance. The inadequacy of the adiabatic potential energy curves to fully explain the vibrational excitation is further emphasized by the strong resonant excitation of a single quantum of the Jahn–Teller inactive C–C–C deformation vibration.

ACKNOWLEDGMENTS

I express my sincere appreciation to Professor E. Haselbach for his continuing support and encouragment in the present work. My thanks go to E. Brosi and P.-H. Chassot, who made a major contribution to the construction of the spectrometer. I thank W. Domcke (Munich) for kind explanations and comments on the manuscript. This work is part of Project 20-34071.92 of the Schweizerischer Nationalfonds zur Förderung der Wissenschaftlichen Forschung.

[1] H. Köppel, L. S. Cederbaum, W. Domcke, and S. S. Shaik, Angew. Chem. **95**, 221 (1983).
[2] H. Estrada, L. S. Cederbaum, and W. Domcke, J. Chem. Phys. **84**, 152 (1986).
[3] L. S. Cederbaum, W. Domcke, and H. Köppel, Chem. Phys. **33**, 319 (1978); C. Woywod and W. Domcke, *ibid.* **162**, 349 (1992).
[4] B. Ciommer, K. M. Nguyen, H. Schwarz, G. Frenking, G. Kwiatkowski, and E. Illenberger, Chem. Phys. Lett. **104**, 216 (1984).
[5] M. Allan, J. Phys. B **25**, 1559 (1992).
[6] O. Schafer, M. Allan, G. Szeimies, and M. Sanktjohanser, J. Am. Chem. Soc. **114**, 8180 (1992).
[7] R. K. Nesbet, Phys. Rev. A **20**, 58 (1979).
[8] J. C. Nickel, P. W. Zetner, G. Shen, and S. Trajmar, J. Phys. B **22**, 730 (1989).
[9] T. Shimanouchi, *Tables of Molecular Vibrational Frequencies* (Natl. Stand. Ref. Data Ser. 39, Natl. Bur. Stand., U.S. Government Printing Office, Washington, D.C., 1972), consolidated Vol. 1.
[10] M. Morrison, Adv. At. Mol. Phys. **24**, 51 (1988).
[11] T. Koopmans, Physica **1**, 104 (1934).
[12] D. Chen and G. A. Gallup, J. Chem. Phys. **93**, 8893 (1990).
[13] A. Schmelzer and E. Haselbach, Helv. Chim. Acta **54**, 1299 (1971); improved and modernized version of T. Bally, S. Matzinger, and B. Albrecht.
[14] A. Herzenberg, in *Electron–Molecule Collisions*, edited by I. Shimamura and K. Takayanagi (Plenum, New York, 1984).
[15] P. D. Burrow, J. A. Michejda, and K. D. Jordan, J. Chem. Phys. **86**, 9 (1987).
[16] M. J. Frisch, G. W. Trucks, M. Head-Gordon, P. M. W. Gill, M. W. Wong, J. B. Foresman, B. G. Johnson, H. B. Schlegel, M. A. Robb, E. S. Replogle, R. Gomperts, J. L. Andres, K. Raghavachari, J. S. Binkley, C. Gonzalez, R. L. Martin, D. J. Fox, D. J. Defrees, J. Baker, J. J. P. Stewart, and J. A. Pople, Gaussian 92, Gaussian, Inc., Pittsburgh, PA, 1992, revision C.
[17] L. Dubé and A. Herzenberg, Phys. Rev. A **11**, 1314 (1975).
[18] L. S. Cederbaum and W. Domcke, Z. Phys. A **277**, 221 (1976).